Journal of Medicinal Chemistry



Article

# Discovery of Hydrocarbon-Stapled Short #-Helical Peptides as Promising Middle East Respiratory Syndrome Coronavirus (MERS-CoV) Fusion Inhibitors

Chao Wang, Shuai Xia, Peiyu Zhang, Tianhong Zhang, Weicong Wang, Yangli Tian, Guangpeng Meng, Shibo Jiang, and Keliang Liu

*J. Med. Chem.*, **Just Accepted Manuscript** • DOI: 10.1021/acs.jmedchem.7b01732 • Publication Date (Web): 14 Feb 2018



## Just Accepted



ACS Publications

Journal of Medicinal Chemistry is published by the American Chemical Society. 1155 Sixteenth Street N.W., Washington, DC 20036

# Discovery of Hydrocarbon-Stapled Short α-Helical Peptides as Promising Middle East Respiratory Syndrome Coronavirus (MERS-CoV) Fusion Inhibitors

*Chao Wang,*[†,¶] *Shuai Xia,*[‡,¶] *Peiyu Zhang,*[#,¶] *Tianhong Zhang,*[†] *Weicong Wang,*[‖] *Yangli Tian,*[†] *Guangpeng Meng,*[#] *Shibo Jiang*[*,‡,§] *and Keliang Liu*[*,†,#]

[†]State Key Laboratory of Toxicology and Medical Countermeasures, Beijing Institute of Pharmacology & Toxicology, 27 Tai-Ping Road, Beijing 100850, China;

[‡]Key Laboratory of Medical Molecular Virology of MOE/MOH, School of Basic Medical Sciences & Shanghai Public Health Clinical Center, Fudan University, 130 Dong An Road, Shanghai 200032, China;

[#]Key Laboratory of Structure-based Drug Design & Discovery of the Ministry of Education, Shenyang Pharmaceutical University, Shenyang 110016, China;

[§]Lindsley F. Kimball Research Institute, New York Blood Center, New York, NY 10065, USA;

[‖]Pharmaceutical Preparation Section, Plastic Surgery Hospital, Chinese Academy of Medical Sciences and Peking Union Medical College, Beijing 100144, China

[¶]These authors contributed equally to this work.

**Abstract**

The hexameric α-helical coiled-coil formed between the C-terminal and N-terminal heptad repeat (CHR and NHR) regions of class I viral fusion proteins plays an important role in mediating the fusion of the viral and cellular membranes and provides a clear starting point for molecular mimicry that drives viral fusion inhibitor design. Unfortunately, such peptide mimicry of the short α-helical region in the CHR of Middle East respiratory syndrome coronavirus (MERS-CoV) spike protein has been thwarted by the loss of the peptide's native α-helical conformation when taken out of the parent protein structure. Here, we describe that appropriate all-hydrocarbon stapling of the short helical portion-based peptide to reinforce its bioactive secondary structure remarkably improves antiviral potency. The resultant stapled peptide P21S10 could effectively inhibit infection by MERS-CoV pseudovirus and its spike protein-mediated cell-cell fusion; additionally, P21S10 exhibits improved pharmacokinetic properties than HR2P-M2, suggesting strong potential for development as an anti-MERS-CoV therapeutic.

## Introduction

Class I viral fusion proteins, such as those of the corona-, retro-, filo-, orthomyxo-, and paramyxoviruses, share similarities in their apparent use of a trimer of α-helical hairpins, or six-helix bundle (6-HB), to mediate membrane fusion processes of virus to target cell.[1,2] In the 6-HB viral fusion apparatus, the C-terminal heptad repeat (CHR) segment of the trimeric virus glycoproteins zips up into three α-helices along the conserved hydrophobic grooves on the periphery of an internal three-stranded coiled coil formed by the N-terminal heptad repeat (NHR) region of those fusion proteins.[3, 4] Despite the topologically similar conformation of the fusion-promoting hexameric helical scaffold, their α-helical portion of the CHR domain displays dramatic differences in length. For example, the fusion core structure of HIV, a *Retroviridae* family member, contains regular α-helical CHR domains involving approximately 10 helical turns that bind to the central trimeric NHR helices.[5,6] In contrast, some other class I enveloped viruses, including Middle East respiratory syndrome coronavirus (MERS-CoV) of the *Coronaviridae* family, encode a notable dimorphism in the length of its NHR and CHR helices.[7-10] In the MERS-CoV 6-HB assembly, the NHR trimers have ~21 helical turns, whereas the central CHR helices are limited to ~4.5 turns within the longer heptad-repeat sequence (Figure 1A).[11]

Blocking α-helix-mediated NHR/CHR interactions using CHR-derived peptides that target the transiently exposed NHR coiled coil is a promising approach to inhibit membrane fusion and viral infection.[12,13] With this strategy, a family of decoy α-helices structurally mimicking the lengthy C-terminal helices of HIV was identified as low-nanomolar inhibitors of viral entry.[14,15] It was disappointing that a synthetic peptide spanning the α-helical region of the MERS-CoV CHR domain sequence showed no anti-MERS-CoV activity.[11, 16] Although the typical α-helical

region is an important recognition motif for MERS-CoV fusion core formation, this short CHR peptide alone does not retain its native conformation owing to the lack of structural reinforcement provided by the parent protein, which, in turn, retards its binding to partner NHR helices.[11]

Peptide stapling based on different macrocyclization chemistry is a key technique for constraining short peptides in α-helical structures and thereby pre-organizing them into their bound conformations to modulate helix-mediated protein-protein interactions with reduced entropic penalty.[17,18] Among numerous stapling chemistries, ruthenium-catalyzed RCM is one of the most noteworthy methods.[19,20] This method of producing all-hydrocarbon-stapled α-helical peptides affords high levels of α-helix induction and nucleation, thus directly resulting in peptide target-binding proclivity, cell permeability, and serum stability.[21,22] Furthermore, the therapeutic potential of stapled peptides has been showcased in a growing diversity of biological settings. Two hydrocarbon-stapled peptides developed by Aileron Therapeutics have reached clinical trials, epitomizing the early indications regarding the clinical translational potential of these stabilized α-helical peptidomimetics.[23, 24]

In the present study, we employed hydrocarbon stapling to recapitulate the topography of α-helical motifs found in the MERS-CoV CHR region to inhibit MERS-CoV infection and its spike (S) protein-mediated cell-cell fusion. In the process of developing these stapled α-helical peptides, we performed a detailed study to identify the optimal stapling sites and the effect of hydrophobic amino acid incorporation to generate promising therapeutics.

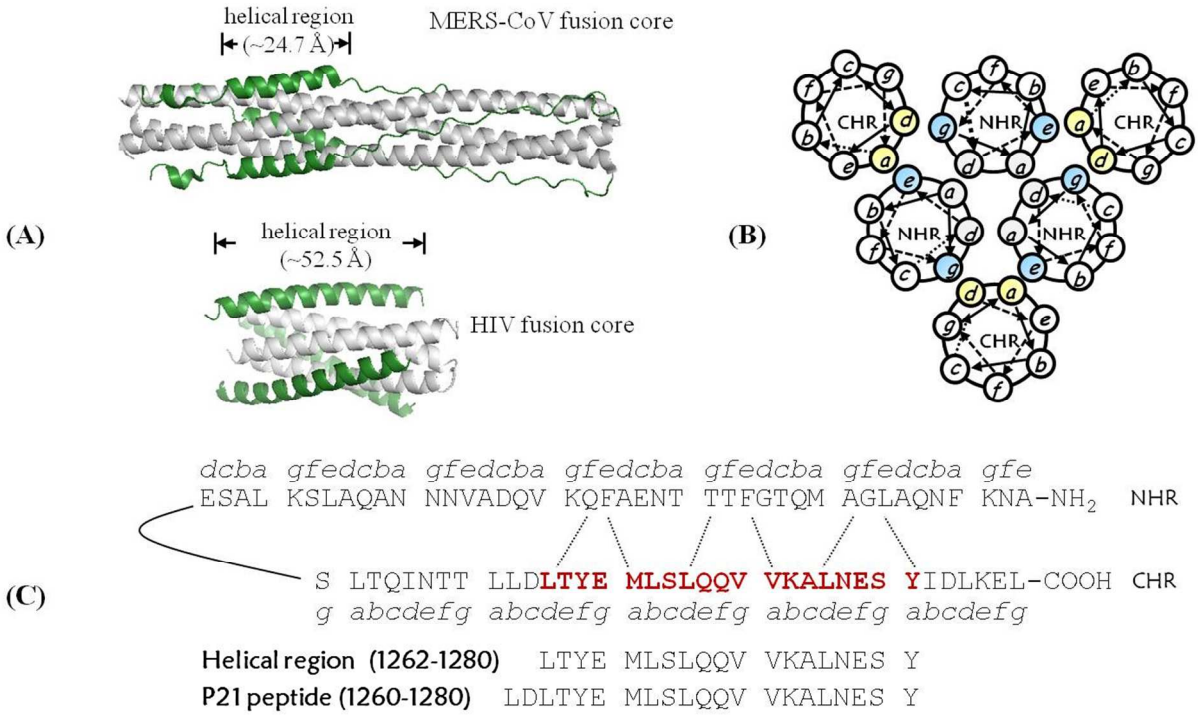


**Figure 1.** Crystal structure of the MERS-CoV six-helix bundle (6HB) fusion core and the design of peptides based on the interaction between the NHR and CHR domains. (**A**) Cartoon representations of the MERS-CoV and HIV 6HBs, in which the NHR trimers and CHR segments are colored in grey and green, respectively. In the HIV 6HB structure (PDB code: 1AIK), the CHR segments form regular helices that pack against the central NHR core. In contrast, only a short helical domain is found within the MERS-CoV CHR (PDB code: 4NJL). (**B**) Helical wheel representation of the 6HB. In the CHR, the residues at the *a-d* positions (yellow) in direct contact with the NHR domains are buried in the 6HB. (**C**) Interaction between the NHR and CHR peptides, as well as the designed P21 peptide. The dashed lines between the NHR and CHR domains indicate the interaction between the residues located at the *a-d* positions in the CHR and the *e-g* positions in the NHR to form the 6HB. The helical domain sequence in MERS-CoV CHR is highlighted in red.

## Design

The primary structure of the MERS-CoV S protein hexameric coiled-coil fusion complex exhibits a heptad repeat pattern usually denoted as *a-b-c-d-e-f-g*.[11, 16] In structural terms, three NHR helices form a trimeric coiled-coil inner core using their *a-d* residues for self-association,

while those at the *e-g* positions participate in the interhelical knob-in-hole packing interaction with residues at the *a-d* positions of CHR helices, which are considered critical for stabilizing the 6-HB structure (Figure 1B).[25, 26] According to the crystal structure of the MERS-CoV fusion core, residues L1262 at position *d* to Y1280 at position *a* in the CHR domain adopt a canonical α-helical region, binding to the deep grooves of the NHR trimers. Seminal work investigating the stability of the coiled coil suggests that helices consisting of fewer than three heptads generally do not create enough opportunities for hydrophobic interactions in the core to favor superhelical assembly.[27,28] Based on the X-ray crystallography and coiled-coil sequence-to-structure relationship study, we engineered a peptide containing the three integral heptads, designated as P21, spanning residues 1260–1280 of the MERS-CoV S protein CHR, as a template for inhibitor design (Figure 1C). Analysis of the crystal structure of CHR in complex with NHR helices shows that six residues at the *a* and *d* positions (L1262, M1266, L1269, V1273, L1276, and Y1280) are buried in the 6-HB. In addition to the hydrophobic interactions contributed by their side chains, residues L1262, M1266, V1273, and Y1280 form four hydrogen bonds with NHR-helical trimer residues, including Q1023, N1016, Q1009, and K1000, via their main-chain amino or oxygen groups. Meanwhile, the hydroxyl group of the Y1280 side chain accepts a hydrogen bond from the NH group of Q1009 in NHR-helices.[11,16] Together with critical hydrophobic stacking forces, these hydrogen bonds constitute a polar contact network that further tightly ties CHR to NHR helix. We initially utilized the "staple scanning" approach along the length of the peptide helix, but away from the critical *a-d* residues, to identify the optimal stapling sites. We substituted pairs of (*S*)-2-(4-pentenyl)alanine (abbreviated as S5 residues) at the *i* and *i+4* positions, since it is the most widely used unnatural amino acid for such type of staple.[21] Accumulated evidence that underline the structure and stability of coiled-coils has shown that the

superhelix stability can generally be improved by inserting residues with more hydrophobic side-chains at the *a-d* positions. [28,29] Among the six buried *a-d* residues, Leu and Val, who possess high hydropathy indices,[30] can strongly bind to the grooves on the surface of the N-helix trimer through their fully hydrophobic side chain interactions but Met and Tyr are polar residues. Based on the scanning study results, we elected to create stapled structures with hydrophobic mutations in the buried *a-d* residues through individual substitution of M1266 or Y1280 with L-norleucine, an isosteric Met analogue with less polar and more hydrophobic properties,[31] or F, respectively, or a combination of both replacements, thus expecting to form a potential hydrophobic binding core.

## Results and Discussion

**Effect of stapling on inhibition of MERS-CoV S protein-mediated cell-cell fusion.** First, peptides P21S1–P21S10 were tested for their ability to inhibit MERS-CoV fusion with its target cell using our previously developed MERS-CoV S protein-mediated cell-cell fusion assay.[11] As shown in Table 1, the linear wild-type P21 exhibited no inhibition at a concentration of up to 50 μM, but when the peptides were cyclized, markedly improved inhibitory activity was demonstrated. Among these α-helical mimetics, P21S8 and P21S10 strongly inhibited S protein-mediated cell-cell fusion, with $EC_{50}$ values of 0.26 μM and 0.33 μM, respectively, which are even more potent than the most active MERS-CoV fusion inhibitor so far, namely the 36-mer peptide HR2P-M2.[11] Importantly, their unmetathesized analogs, i.e., peptides containing uncrosslinked S5 residues, had a dramatically decreased membrane fusion inhibitory potency (Table 1). These results reveal the critical contribution of hydrocarbon stapling to replicate the local topography of MERS-CoV short C-terminal helices for therapeutic benefit. In addition, shifting the position of the all-hydrocarbon staple had a significant effect on anti-MERS-CoV

activity. Peptides P21S2, P21S4, P21S5, and P21S9, with a 2/6, 5/9, 8/12, and 15/19 staple, respectively, exhibited only similar activity compared to their relevant unstapled peptides whereas peptides P21S1, P21S3, P21S6, and P21S7 had no activity. Compared to P21S8 whose cross-link had the *S*,*S*-configuration, its *R*,*R*-configured counterpart, P21R8, provided 62-fold weaker anti-MERS-CoV activity, consistent with previous publications revealing the requirement of *S*-form building blocks for an *i*, *i+4* staple type.[21] Finally, we explored whether the incorporation of hydrophobic mutations at the binding interface could lead to an improvement in biological activity. In our assay, replacing M1266 with L-norleucine (i.e., Z), which led to P21S8Z, retained the high activity of P21S8 whereas Y1280F alone and the combination of M1266Z and Y1280F showed decreased potencies compared to that of P21S8, indicating the critical role of hydrogen bond formation between Y1280 and Q1009 of the S protein NHR trimer. Although buried hydrophobic residues may contribute more energy toward stabilization of a coiled-coil structure than polar interactions,[28, 32] subtle specific interacting networks are required for hydrocarbon-stapled peptides to stop the MERS-CoV–cell fusion process efficiently.

**Table 1.** Inhibitory Activities of Stapled Peptides on MERS-CoV S Protein-Mediated Cell-Cell Fusion

| Compound | Sequence[a] | $EC_{50}$ (μM)[e] |
|---|---|---|
| | Hydrocarbon Stapled Peptides[b] | |
| P21S1 | *****DLT*****EM LSLQQVV KALNESY | >50 |
| P21S2 | L*****LTY*****M LSLQQVV KALNESY | 3.90 ± 1.1 |
| P21S3 | LDL*****YEM *****SLQQVV KALNESY | >50 |
| P21S4 | LDLT*****EM L*****LQQVV KALNESY | 7.14 ± 0.7 |
| P21S5 | LDLTYEM *****SLQ*****VV KALNESY | 10.7 ± 2.6 |
| P21S6 | LDLTYEM L*****LQQ*****V KALNESY | >50 |
| P21S7 | LDLTYEM LSL*****QVV *****ALNESY | >50 |
| P21S8 | LDLTYEM LSLQ*****VV K*****LNESY | 0.26 ± 0.05 |
| P21S9 | LDLTYEM LSLQQVV *****ALN*****SY | 14.1 ± 2.3 |
| P21S10 | LDLTYEM LSLQQVV K*****LNE*****Y | 0.33 ± 0.04 |
| | Unstapled Peptides[c] | |
| P21L2 | L**X**LTY**X**M LSLQQVV KALNESY | 10.9 ± 1.1 |
| P21L4 | LDLT**X**EM L**X**LQQVV KALNESY | 8.21 ± 0.9 |
| P21L5 | LDLTYEM **X**SLQ**X**VV KALNESY | 4.49 ± 0.6 |
| P21L8 | LDLTYEM LSLQ**X**VV K**X**LNESY | 20.6 ± 3.3 |
| P21L9 | LDLTYEM LSLQQVV **X**ALN**X**SY | 10.9 ± 1.0 |
| P21L10 | LDLTYEM LSLQQVV K**X**LNE**X**Y | 3.55 ± 0.2 |
| | P21S8 Mutated Peptides[d] | |
| P21R8 | LDLTYEM LSLQ^VV K^LNESY | 16.3 ± 1.1 |
| P21S8Z | LDLTYE**Z** LSLQ*****VV K*****LNESY | 0.63 ± 0.05 |
| P21S8F | LDLTYEM LSLQ*****VV K*****LNES**F** | 2.16 ± 1.1 |
| P21S8ZF | LDLTYE**Z** LSLQ*****VV K*****LNES**F** | 3.89 ± 0.8 |
| | Control Peptides | |
| P21 | LDLTYEM LSLQQVV KALNESY | >50 |
| HR2P-M2 | SLTQINTTLLDLEYEMKKLEEVVKKLEESYIDLKEL | 0.75 ± 0.09 |

[a] These peptides have an acetyl group at the N-terminus and carboxyamide at the C-terminus. [b] Asterisks indicate the positions of the S5 residues, which react to form the all-hydrocarbon staple. [c] X indicates the positions of the S5 amino acids left uncyclized. [d] ^ denotes the positions of the R5 amino acids, which react to form staples. [e] $EC_{50}$ data were derived from the results of three independent experiments and are expressed as the mean ± standard deviation.

**Stapled peptides as inhibitors of pseudotyped MERS-CoV infection.** Subsequently, we tested the potential inhibitory activities of the P21S8, P21S10, and P21S8Z peptides, which exhibited promising inhibitory potency in the cell-cell fusion assay, on MERS-CoV pseudovirus infection

in Huh-7 cells. As shown in Table 2 and Figure S1, P21S8, P21S10, and P21S8Z could significantly inhibit the MERS-CoV pseudovirus carrying the wild-type S protein, with $EC_{50}$ values of 3.03, 0.97, and 2.80 μM, respectively. Although P21S8 exhibited 2.8-fold greater potency than the positive control HR2P-M2 in inhibiting cell-cell fusion, it was 2.8-fold less active than HR2P-M2 against wild-type MERS-CoV pseudovirus. Notably, P21S10 displayed potency similar to that of HR2P-M2 in both cell-cell and virus-cell fusion inhibition. These results suggest that, unlike P21S10, P21S8 does not have good correlation between its blockage of S protein-mediated membrane fusion and inhibition of wild-type MERS-CoV infection. One of the possible explanations for this discrepancy is that P21S8 may have lower target binding capability than P21S10 during the inhibition of virus infection. In addition, none of these viral fusion blockers displayed significant cytotoxicity to Huh-7 cells up to 100 μM (Table 2 and Figure S2). The selectivity index ($SI=CC_{50}/EC_{50}$) of P21S10 was greater than 103. Among clinical MERS-CoV strains, S protein amino acid changes of Q1020H and Q1020R located in the NHR domain were under positive selection and present in nearly all variants.[33] Therefore, we next investigated whether P21S8, P21S10, and P21S8Z would be effective against MERS-CoV strains with the Q1020H and Q1020R mutations. Strikingly, these peptides were effective for inhibiting infection by MERS-CoV pseudoviruses with mutated S protein, with $EC_{50}$ values similar to those for inhibiting pseudovirus carrying the wild-type S protein (Table 2 and Figure S1). P21S8 and P21S8Z displayed about 3-fold less potency than HR2P-M2 for inhibiting infection by pseudoviruses carrying S protein with Q1020H or Q1020R mutation; however, P21S10 possessed potency similar to that of HR2P-M2. Since MERS-CoV is primarily infecting the human respiratory tract, we further tested the inhibitory activities of these stapled peptides on MERS-CoV pseudovirus infection in a human lung-derived cell line Calu-3. Strikingly, P21S8,

P21S10, and P21S8Z could inhibit MERS-CoV pseudovirus infection in Calu-3 cells with $EC_{50}$ values of 2.21, 1.58, and 2.57 μM, respectively, in an agreement with result observed in experiment using Huh-7 cells (Table S1 and Figure S2). They also had no significant cytotoxicity to Calu-3 cells at the concentrations as high as 100 μM (Figure S3). Moreover, we evaluated the aqueous solubility of these stapled peptides. P21S8 and P21S10 had aqueous solubilities of 6.47 mg/mL and 10.5 mg/mL at pH 7.4, respectively, which were 14-fold and 22-fold higher than that of P21S8Z (Table S2), suggesting their good potential for further development.

**Table 2.** Inhibitory activity of P21S8, P21S10, and P21S8Z on infection by pseudotyped MERS-CoV[a]

| Compound | $EC_{50}$ (μM) for inhibiting | | | $CC_{50}$ (μM) | SI[b] |
|---|---|---|---|---|---|
| | WT MERS-CoV pseudovirus | Q1020H-MERS-CoV pseudovirus | Q1020R-MERS-CoV pseudovirus | | |
| P21S8 | 3.03 ± 0.29 | 4.06 ± 0.34 | 1.98 ± 0.28 | >100 | >33 |
| P21S10 | 0.97 ± 0.08 | 1.82 ± 0.28 | 0.89 ± 0.07 | >100 | >103 |
| P21S8Z | 2.80 ± 0.74 | 4.15 ± 0.25 | 2.49 ± 0.18 | >100 | >36 |
| HR2P-M2 | 1.07 ± 0.21 | 1.25 ± 0.18 | 0.64 ± 0.16 | >100 | >93 |

[a] Data were derived from the results of three independent experiments and are presented as the mean ± standard deviation. [b] SI (selectivity index) = $CC_{50}/EC_{50}$ for inhibiting WT MERS-CoV pseudovirus infection.

**Effect of stapling on helical propensity.** Next, we sought to determine whether hydrocarbon stapling could effectively recapitulate the native conformation of the α-helical region in the MERS-CoV CHR domain. CD spectroscopy provides a typical signature for α-helices with a maximum near 190 nm and double minima at 208 and 222 nm. CD spectra showed that P21 displayed a random coil conformation in phosphate buffer. Strikingly, with the exception of P21S2 that was too insoluble to make accurate measurements, the other hydrocarbon-stapled peptides exhibited α-helical structure with 15.6–54.5% helicity. Among them, the highly effective stapled peptides P21S8 and P21S10 were found to have greatly improved helical

propensity, compared to the linear wild-type peptide, with helical contents of 53.7% and 46.5%, respectively (Figure 2). Furthermore, these stapled peptides were indeed more helical than their correponding uncyclized linear precursors (Table S3–S4). These data further confirmed the successful mimicry of the CHR helix via cyclization using the stapling strategy. Interestingly, although the CD spectra for peptides P21S8 and P21S10 were similar to those of P21S6 and P21S7, a difference in inhibitory potency of more than 193-fold was observed between them, suggesting that the much higher biological activity cannot be merely attributed to the helical propensity. Hence, the following target-binding studies were performed to further elucidate their mechanisim of action.

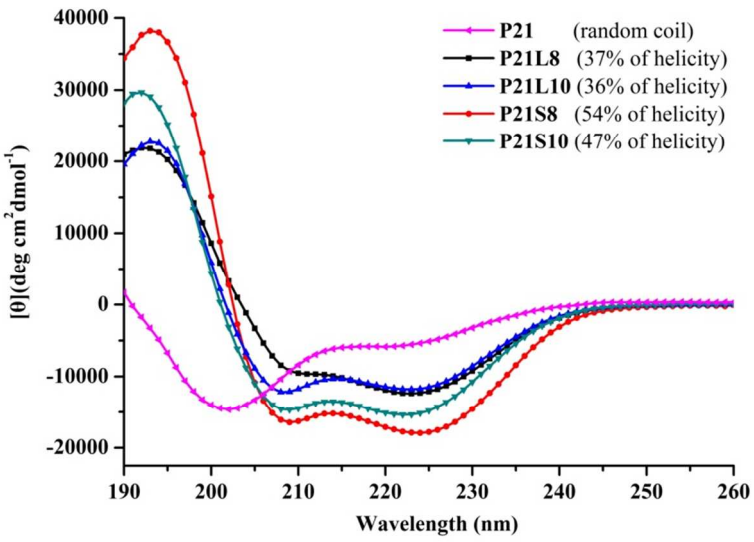


**Figure 2.** CD spectra of the isolated peptides P21S8 and P21S10. The corresponding unstapled counterparts and linear peptide P21 are included for structural comparison. The final concentration of each peptide in PBS (pH 7.2) was 50 μM.

**Binding of stapled peptides to their complementary S protein NHR domain.** Previous studies have shown that peptides derived from the MERS-CoV S protein CHR domain can bind to their NHR target to form a stable α-helix hexamer.[11] Here, we first sought to determine the

interaction of the stapled helical peptides with their native NHR ligand, designated HR1P, to form stable α-helical complexes using CD spectroscopy. The significant increase over the sum of the individual spectra of two peptides mixed together in equimolar concentrations indicates that the interaction between them led to enhanced helical structures.[34, 35] The isolated HR1P displays a random coil structure in phosphate buffer (pH 7.2) as judged by CD spectroscopy, which was consistent with previous reports.[11] Both P21S8 and P21S10 interacted with HR1P, resulting in 35.5% and 45.6% α-helical content in the complex, respectively. The CD signals of the P21S8/HR1P mixture and the P21S10/HR1P mixture at 222 nm were dramatically greater than the mathematical sum of those of the isolated peptides, indicating the induction of a large α-helical structure upon their interaction (Figure 3A). Strikingly, the thermal unfolding transition (*Tm*) values of P21S8/HR1P and P21S10/HR1P reached 71.1 ℃ and 76.4 ℃, respectively (Figure 3B). Together, these CD data are consistent with P21S8/HR1P and P21S10/HR1P folding to form thermally stable and cooperatively folded helical bundles. Stapled peptides with moderate activity, including P21S4, P21S5, and P21S9, resulted in a less stable interaction with *Tm* values ranging from 56.6 ℃ to 66.6 ℃ while peptides with very poor antiviral activity showed no, or weak, coiled-coil interactions (Table S4). These results demonstrated a strong correlation between the biological activities and the thermal stabilities of the stapled peptides/HR1P complexes.

The binding of the stapled peptides to the NHR-derived peptide HR1P was further confirmed using native (N)-PAGE. In N-PAGE, owing to its net positive charge, HR1P did not appear on the gel as it migrated into the solvent under the native electrophoresis conditions; these results are consistent with previous observations.[11] The respective stapled helical peptides with various antiviral potencies were mixed with HR1P and subjected to N-PAGE analysis. As shown

in Figure 3C, both P21S8 and P21S10 formed stable complexes with HR1P, as evidenced by new bands at the upper position in the gel concomitant with the fading or disappearance of the stapled peptide bands, suggesting that oligomeric complexes formed via coiled-coil interactions. The N-PAGE results also indicated a stronger binding of either P21S8 or P21S10 to HR1P than the bindings of P21S4, P21S5, and P21S9 to HR1P, based on the densities of the residue-stapled peptide bands observed in the gel (Figure 3C and Figure S4). Consistent with the cell-cell fusion assay and CD spectroscopy results, the inactive peptide P21S1, P21S3, and P21S6 exhibited no NHR binding. Interestingly, the mixture of P21S7/HR1P did not show new band at the upper position in the gel, while the P21S7 band in the mixture had a much lower intensity than the corresponding P21S7 band alone (Figure S4). This is in agreement with the CD data, where the signal of the P21S7/HR1P mixture was dramatically smaller than that of the mathematical sum of the isolated peptides, suggesting that addition of P21S7 to HR1P distorts the α-helical conformation of P21S7 due to their interaction. The combined CD and N-PAGE data indicate that P21S7 may associate with the viral N-helices to form non-helical complexes or aggregates that cannot migrate in the gel, thus resulting in no inhibitory activity against MERS-CoV infection.

The sizes of the complexes formed between HR1P and P21S8 or P21S10 were further confirmed by sedimentation velocity analysis (SVA). As analyzed by SVA, the sedimentation coefficients of the P21S8/HR1P complex and the P21S10/HR1P complex were 2.27 s and 1.94 s, corresponding to 22.6 kDa and 22.3 kDa, respectively. Compared to the expected molecular masses of 7.07 kDa for the P21S8/HR1P heterodimer and 7.10 kDa for the P21S10/HR1P heterodimer, we concluded that P21S8 and P21S10 could both associate with HR1P to form a

heterogeneous 6HB complex, thus blocking MERS-CoV entry into the host cells (Figure 3D and Table S5).

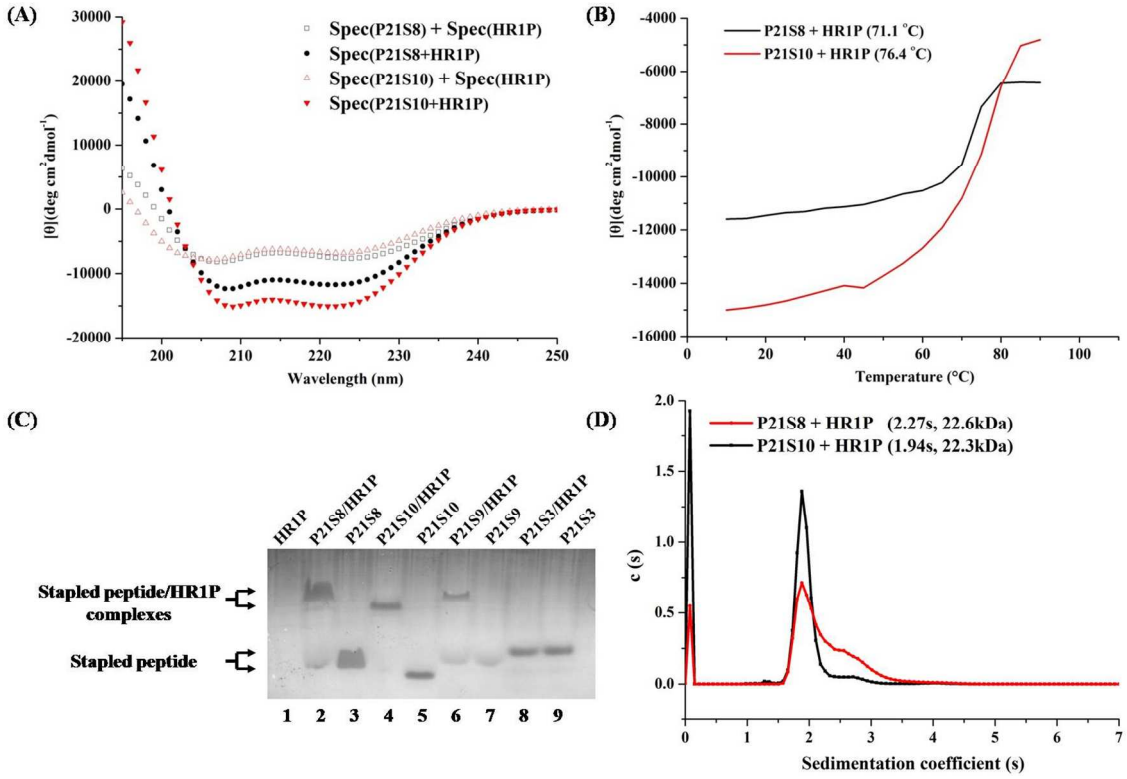


**Figure 3.** Binding of P21S8 and P21S10 to the NHR peptide HR1P. (**A**) CD spectrum of peptide mixtures (Spec(C+N), solid symbols) and the sum of the spectra of the related isolated peptides (Spec(C) + Spec(N), open symbols) are shown for comparison. The hydrocarbon-stapled peptide/HR1P interaction induces more α-helix content than the sum of the single peptides. The final concentration of each peptide in PBS was 50 μM. (**B**) The thermostability of the complexes formed by P21S8 or P21S10 and the target mimic NHR peptide HR1P was determined by CD spectroscopy. The final concentration of each peptide in PBS was 50 μM. (**C**) N-PAGE analysis of the stapled peptides, HR1P, and their complexes. Lane 1: HR1P, lane 2: P21S8 + HR1P, lane 3: P21S8, lane 4: P21S10 + HR1P, lane 5: P21S10, lane 6: P21S9 + HR1P, lane 7: P21S9, lane 8: P21S3 + HR1P, lane 9: P21S3. (**D**) Sedimentation velocity analysis of the P21S8/HR1P mixture and the P21S10/HR1P mixture. The sedimentation coefficient (s) and the observed molecular mass (kDa) of each peak are indicated in parentheses.

**Pharmacokinetic studies.** The pharmacokinetic behavior of P21S10, P21S8, and HR2P-M2 was comparatively evaluated in rats. Sprague-Dawley rats (200 ± 10 g) were injected intravenously with the three peptides (4 mg/kg). Seven blood samples were collected sequentially over a 240-min period (three animals at each time point), and the concentrations of the intact peptides in plasma were determined by LC/MS/MS analysis. As shown in Figure 4 and Table 3, although these three peptides exhibited similar *in vivo* half-lives, the mean value of the maximum blood concentration ($C_{max}$) for P21S10 was 3.6–5.8-fold greater than those for P21S8 and HR2P-M2. Meanwhile, we observed dramatic differences among the areas under the plasma concentration–time curve extrapolated to the last time point ($AUC_{0-t}$), a measure of the total systemic exposure to a drug, for the three compounds. The $AUC_{0-t}$ was 91.3 μg/(mL·h) for P21S10 as compared to 44.1 μg/(mL·h) for P21S8 and 3.36 μg/(mL·h) for HR2P-M2. Consequently, P21S10 showed the lowest systemic clearance (0.041 (L/h)/kg), which was approximately 25-fold less than that of HR2P-M2 (1.04 (L/h)/kg). Thus, the current results indicate that P21S10 should be further developed as a potential drug candidate on the basis of its high potency in inhibiting infection of divergent MERS-CoV strains and its improved pharmacokinetics compared with HR2P-M2.

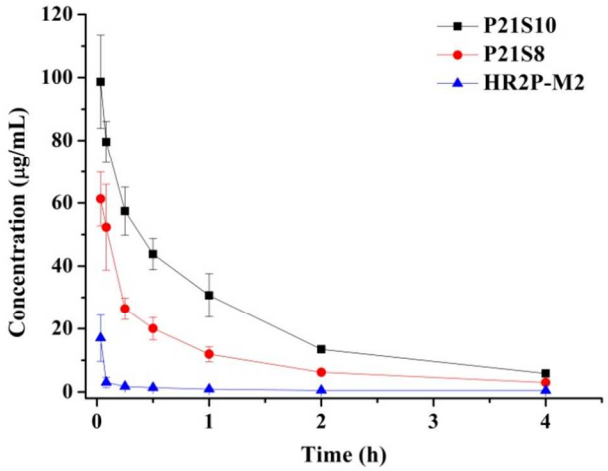


**Figure 4.** Pharmacokinetic profiles of P21S10, P21S8, and HR2P-M2 in plasma following the administration of a single intravenous dose (4 mg/kg) to Sprague-Dawley rats (n=3).

**Table 3.** Pharmacokinetic parameters of P21S10, P21S8, and HR2P-M2 in rats following a single dose i.v. administration calculated by noncompartmental analysis by using DAS, version 3.2.8.[a]

| Compd | AUC (0–t) (μg/(mL • h)) | MRT (0-t) (h) | $t_{1/2}$ (h) | CL ((L/h)/kg) | $C_{max}$ (μg/mL) | $V_d$ (L/kg) |
|---|---|---|---|---|---|---|
| P21S10 | 91.3 ± 9.8 | 1.08 ± 0.04 | 1.15 ± 0.15 | 0.041 ± 0.006 | 98.7 ± 6.5 | 0.066 ± 0.004 |
| P21S8 | 44.1 ± 1.0 | 1.03 ± 0.04 | 1.32 ± 0.49 | 0.082 ± 0.004 | 61.8 ± 13.6 | 0.156 ± 0.052 |
| HR2P-M2 | 3.35 ± 0.5 | 1.34 ± 0.14 | 1.54 ± 0.73 | 1.04 ± 0.26 | 17.0 ± 1.3 | 2.188 ± 0.603 |

[a] MRT, mean residence time; CL, clearance; $C_{max}$, maximum drug concentration; $V_d$, volume of distribution.

## Conclusions

We provide the first example of all-hydrocarbon-stapled peptides mimicking the native conformation of the C-terminal short α-helical region within the MERS-CoV S protein. These stapled peptides were able to block the formation of the hexameric coiled-coil fusion complex and thus inhibit viral–host cell membrane fusion. Our data showed that one of these stapled peptides, P21S10, not only preserves the biologically active α-helical conformation, as found in the MERS-CoV fusion machinery, but also has good potential to be developed into anti-MERS therapeutics based on its promising antiviral activity, effective native ligand-binding capability, and favorable pharmacokinetics. Formation of MERS-CoV 6-HB fusion core between CHR and NHR is basically the result of α-helix-mediated protein-protein interactions wherein the CHR helix can be considered to have two distinct faces, *i.e.*, a buried hydrophobic surface and a solvent-exposed surface.[29] The established rules of thumb that underline the sequence and structure in coiled coils reveal that stabilization of individual helices will enhance the overall stability of the superhelical protein structural motif.[28] Therefore, strategies used for reinforcing the secondary structure of constituent α-helices in a coiled coil such as introducing intrahelical salt bridges at solvent accessible site and substitution of non-core residues with helix-favoring amino acids have been successfully applied to HIV fusion inhibitor design.[36] We envisioned that these strategies would also be applicable to the further optimization of our lead compounds

found in this study. In addition, rather than generating hydrophobic mutations in buried residues, for future design one should also consider the place of polar amino acids at the interactive site of stapled peptides, which could establish attractive interhelical electrostatic interactions or hydrogen bonds, thus increasing their aqueous solubility and target-binding affinity.[37,38] Overall, considering the universal 6HB fusion mechanism employed by the class I enveloped viruses, our study establishes the paradigm that hydrocarbon stapling may be an attractive strategy for developing viral entry inhibitors designed to control viral epidemics through recapitulating certain α-helical peptides of the viral fusion core structures so that NHR/CHR coiled coil-mediated interactions are inhibited.

## Experimental Section

**General peptide synthesis.** Peptides were prepared using a CEM Liberty automated microwave peptide synthesizer together with the Fmoc solid phase peptide synthesis protocol on Rink-Amide resin with a loading capacity of 0.44 mmol/g. Briefly, the Fmoc protecting group of the resin was removed with 20% piperidine/DMF (2 × 30 min). Natural amino acids were coupled using *O*-benzotriazol-1-yl-*N,N,N',N'*-tetramethyl-uronium hexafluorophosphate (3 equiv) in DMF and diisopropylethylamine (DIEA) (6 equiv) in NMP as coupling reagents, 3 equiv of $N^{\alpha}$-protected amino acid, and 3 equiv of 1-hydroxy-benzotriazole. After each coupling, or Fmoc removal, the resin was washed with DMF (5 × 1 min) and DCM (3 × 1 min). For the assembly of olefin-containing amino acids, a double coupling method was performed to achieve a complete reaction, as described previously.[39] After final deprotection, the peptide-bound resin was treated with acetic acid anhydride-DIEA (1:1, v/v) (2 × 30 min). For synthesis of the all-hydrocarbon-stapled peptides, the RCM reactions of the protected peptides containing S5 ((*S*)-2-(4-pentenyl)alanine) or R5 ((*R*)-2-(4-pentenyl)alanine) were performed on-resin using the First-Generation Grubbs catalyst. First, the reaction bottle containing peptide-bound resin was kept under lucifugal conditions by silver paper and then protected under nitrogen. Second, Grubbs I catalyst (0.3 equiv) in dichloroethane was added to the resin, the mixture was stirred for 6 h

at room temperature, and then repeated treatments with fresh catalyst were carried out for 6 h to obtain more complete conversion. After the reaction solution was drained, the resin was washed with DMF (2 × 1 min) and DCM (2 × 1 min). The resin cleavage was performed by treatment with a cleavage cocktail containing 85% TFA, 5% thioanisole, 5% *m*-cresol, and 5% water. After cleavage from resin, crude peptides were precipitated using cold diethyl ether. The crude products were purified by preparative reversed-phase (RP) HPLC and the purity of each compound was confirmed to be ≥95% by analytical RP-HPLC. Such information is provided in the Supporting Information (Tables S6–S7). The molecular weight of the peptides was confirmed by Q-FT-ICR-MS (Apex Qe, Bruker, Germany).

**Inhibition of MERS-CoV S-protein-mediated cell-cell fusion assay.** MERS-CoV S protein-mediated cell-cell fusion was assessed, as described previously.[40,41] In brief, 293T cells expressing MERS-CoV S protein and enhanced GFP (EGFP) were used as the effector cells (293T/MERS/EGFP), and Huh-7 cells expressing the MERS-CoV receptor DPP4 were used as the target cells. 293T/EGFP cells, which express only EGFP, were used as negative control cells. Huh-7 cells were plated in a 96-well plate ($5 \times 10^4$ per well) and cultured at 37 °C for 5 h. Inhibitors at the indicated concentrations were then added, followed by the addition of 293T/MERS/EGFP cells or 293T/EGFP cells ($1 \times 10^4$ per well). After coculture at 37 °C for 4 h, the 293T/MERS/EGFP cells and 293T/EGFP cells fused or unfused with Huh-7 cells were counted under an inverted fluorescence microscope (Nikon Eclipse Ti-S).

**Inhibition of pseudotyped MERS-CoV infection.** MERS pseudovirus was generated via cotransfection of 293T cells with the plasmid pNL4-3.luc.RE as well as the pcDNA3.1-MERS-CoV-S plasmid, as previously described.[42] Peptides at graded concentrations were mixed with the pseudovirus and then incubated for 1 h at room temperature. The mixture was added to Huh-7 or Calu-3 cells, fresh medium was added 12 h later, and the cells were incubated for an additional 48 h at 37 °C. Fluorescence was determined immediately using a luciferase kit (Promega) and an Ultra 384 luminometer (Tecan) after the addition of luciferase substrate (Promega).

**Cytotoxicity assessment.** The cytotoxicity of compounds on Huh-7 cells used for testing pseudotyped MERS-CoV infection was measured using a Cell Counting Kit (CCK-8, Dojindo, Kumamoto, Japan). Briefly, 5 μL of test peptide at graded concentrations were added to 100 μL of cells ($1 \times 10^5$ per well) in wells of a 96-well plate incubated at 37 °C for 12 h before the addition. After incubation at 37 °C for 48 h, 100 μL of CCK-8 were added. The absorbance at 450 nm was measured 2 h later.

**Aqueous solubility determination.** Solubility was measured by using an HPLC-UV method. Stapled peptides (~2 mg) were added to 1.5-mL Eppendorf tubes and either pH 7.4 phosphate buffer (100 μL) or double-distilled $H_2O$ ($ddH_2O$) (100 μL) was added for dissolution with shaking for 24 h at 25 °C, followed by centrifugation of the mixture at 10,000 rpm for 15 min. The saturated supernatant solution was filtered through a 0.45-μm filter membrane and then transferred to other vials for analysis by HPLC with UV detection. Each sample was assayed in triplicate. For quantification, analytical RP-HPLC was used with a Zorbax Eclipse XDB-C8 column (4.6 mm × 150 mm, 5 μm). Solvent A: 0.1% TFA in $H_2O$; Solvent B: 0.1% TFA in 70% $CH_3CN/H_2O$; flow rate: 1 mL/min; gradient: 5–100% solvent B in solvent A over 25 min. The aqueous concentration was determined by comparison of the peak area of the saturated solution with a standard curve plotted for the peak area versus known concentrations, which was prepared by solutions of test compound in PBS or $ddH_2O$ at 20, 10, 5, 2.5, 0.5, and 0.05 mg/mL.

**CD spectroscopy.** Peptides were dissolved in PBS (50 mM, pH = 7.2) to a final concentration of 50 μM. Equimolar mixtures of HR1P and test peptides were incubated at 25 °C for 30 min at a concentration of 50 μM. The CD spectra were obtained on a Chirascan Plus spectropolarimeter (Applied Photophysics Ltd., Leatherhead, Surrey, UK) at 4 °C. The measurement parameters were set up as follows: wavelength, 190–260 nm; step resolution, 0.5 nm; speed, 20 nm/min. The CD data are shown as the mean residue ellipticity, and the $[\theta]_{222}$ value of -33,000 deg $cm^2$/dmol was taken to correspond to 100% α-helicity. Thermal denaturation was monitored at 222 nm by implementation of a thermal gradient of 2 °C/min from 10 °C to 90 °C.

**N-PAGE.** Stapled peptides and HR1P were dissolved in 50mM PBS and $ddH_2O$ at a concentration of 200 μM, respectively. Each stapled peptide was incubated with HR1P at 25 °C for 30 min, respectively. After the

addition of Tris-glycine native sample buffer (BioRad, Hercules, CA), the samples were loaded onto an 18% Tris-glycine gel with a Tris-glycine sample buffer (pH 8.3). Gel electrophoresis was carried out at a constant voltage of 120 V at room temperature for 3 h, and then the gel was stained with Coomassie blue R250. The images were obtained by the ChampGel 6000 Imaging System (SageCreation Ltd., Beijing, China).

**SVA.** SVA was performed using a ProteomelabTMXL-A/XL-I analytical ultracentrifuge (Beckman Coulter, Fullerton, CA) equipped with a three-channel cell in an An-60 Ti rotor. All samples were prepared at a final concentration of 250 μM in 50 mM PBS. The HR1P/P21S8 and HR1P/P21S10 mixtures were incubated at 25 °C for 30 min and were initially scanned at 3000 rpm for 10 min. Data were obtained at 60,000 rpm at a wavelength of 280 nm and 20 °C for 7 h. Weight-averaged molecular weights were calculated and fitted by processing with the SEDFIT program.

**Pharmacokinetic assessments.** Sprague-Dawley rats weighing 200 ± 10 g each were obtained from the Animal Center of Beijing Institute of Pharmacology & Toxicology and were used for pharmacokinetic assessments. Animals were treated in accordance with the Animal Welfare Act and the "Guide for the Care and Use of Laboratory Animals" (NIH Publication 86-23, revised 1985). Complete pharmacokinetic experimental procedures are provided in the Supporting Information.

## ASSOCIATED CONTENT

**Supporting Information Available**: Tables S1–S7, Figure S1–S4, pharmacokinetic experiments, as well as HPLC purity and characterization data of compounds. This material is available free of charge via the Internet at http://pubs.acs.org.

## AUTHOR INFORMATION

### Corresponding Author

To whom correspondence should be addressed: K.L. and S.J. For K.L.: phone, 86-10-6816-9363; Fax, 86-10-6821-1656, E-mail: keliangliu55@126.com. For S.J.: phone, 86-21-54237673; Fax, 86-21-54237465; E-mail: shibojiang@fudan.edu.cn.

**Author Contributions**

Prof. Keliang Liu, Prof. Shibo Jiang, and Dr. Chao Wang conceived and designed the study. Mr. Peiyu Zhang, Mr. Guangpeng Meng, and Ms Yangli Tian performed synthesis. Mr. Shuai Xia performed biological evaluation. Mr. Peiyu Zhang performed biophysical analysis. Dr. Tianhong Zhang and Ms. Weicong Wang analyzed the pharmacokinetics data. The manuscript was written by Dr. Chao Wang.

## ACKNOWLEDGMENT

This research was supported, in part, by grants from the National Science Foundation of China (81573266 and 81590766) and the National Key Research and Development Program of China (2016YFC1201000)

## ABBREVIATIONS USED

CHR, C-terminal heptad repeat; NHR, N-terminal heptad repeat; 6HB, six-helix bundle; Da, Dalton; SVA, sedimentation velocity analysis.

## REFERENCES

(1) Harrison, S. C. Viral membrane fusion. *Nat. Struct. Mol. Biol.* **2008**, *15*, 690-698.

(2) Dimitrov, D. S. Virus entry: Molecular mechanisms and biomedical applications. *Nat. Rev. Microbiol.* **2004**, *2*, 109-122.

(3) Eckert, D. M.; Kim, P. S. Mechanisms of viral membrane fusion and its inhibition. *Annu. Rev. Biochem.* **2001**, *70*, 777-810.

(4) Vigant, F.; Santos, N. C.; Lee, B. Broad-spectrum antivirals against viral fusion. *Nat. Rev. Microbiol.* **2015**, *13*, 426-437.

(5) Lu, M.; Blacklow, S. C.; Kim, P. S. A Trimeric structural domain of the HIV-1 transmembrane glycoprotein. *Nat. Struct. Biol.* **1995**, *2*, 1075-1082.

(6) Lai, W.; Wang, C.; Yu, F.; Lu, L.; Wang, Q.; Jiang, X.; Xu, X.; Zhang, T.; Wu, S.; Zheng, X.; Zhang, Z.; Dong, F.; Jiang, S.; Liu, K. An effective strategy for recapitulating N-terminal heptad repeat trimers in enveloped virus surface glycoproteins for therapeutic applications. *Chem. Sci.* **2016**, *7*, 2145-2150.

(7) Follis, K. E.; York, J.; Nunberg, J. H. Serine-scanning mutagenesis studies of the C-terminal heptad repeats in the SARS coronavirus S glycoprotein highlight the important role of the short helical region. *Virology* **2005**, *341*, 122-129.

(8) Bullough, P. A.; Hughson, F. M.; Skehel, J. J.; Wiley, D. C. Structure of influenza haemagglutinin at the pH of membrane fusion. *Nature* **1994**, *371*, 37-43.

(9) Liu, S.; Xiao, G.; Chen, Y.; He, Y. X.; Niu, J. K.; Escalante, C. R.; Xiong, H.; Farmar, J.; Debnath, A. K.; Tien, P.; Jiang, S. Interaction between heptad repeat 1 and 2 regions in spike protein of SARS-associated coronavirus: implications for virus fusogenic mechanism and identification of fusion inhibitors. *Lancet* **2004**, *363*, 938-947.

(10) Miller, E. H.; Harrison, J. S.; Radoshitzky, S. R.; Higgins, C. D.; Chi, X.; Dong, L.; Kuhn, J. H.; Bavari, S.; Lai, J.; Chandran, K. Inhibition of Ebola virus entry by a C-peptide targeted to endosomes. *J. Biol. Chem.* **2011**, *286*, 15854-15861.

(11) Lu, L.; Liu, Q.; Zhu, Y.; Chan, K.; Qin, L.; Li, Y.; Wang, Q.; Chan, J. F.; Du, L.; Yu, F.; Ma, C.; Ye, S.; Yuen, K.; Zhang, R.; Jiang, S. Structure-based discovery of Middle East respiratory syndrome coronavirus fusion inhibitor. *Nat.Commun.* **2014**, *5*, 3067.

(12) Berkhout, B.; Eggink, D.; Sanders, R. W. Is there a future for antiviral fusion inhibitors? *Curr. Opin. Virol.* **2012**, *2*, 50-59.

(13) Azzarito, V.; Long, K.; Murphy, N. S.; Wilson, A. J. Inhibition of alpha-helix-mediated protein-protein interactions using designed molecules. *Nat. Chem.* **2013**, *5*, 161-173.

(14) Cai, L.; Jiang, S. Development of peptide and small-molecule HIV-1 fusion inhibitors that target gp41. *ChemMedChem* **2010**, *5*, 1813-1824.

(15) Pan, C.; Liu, S.; Jiang, S. HIV-1 gp41 fusion intermediate: a target for HIV therapeutics. *J. Formos. Med. Assoc.* **2010**, *109*, 94-105.

(16) Gao, J.; Lu, G.; Qi, J.; Li, Y.; Wu, Y.; Deng, Y.; Geng, H.; Li, H.; Wang, Q.; Xiao, H.; Tan, W.; Yan, J.; Gao, G. Structure of the fusion core and inhibition of fusion by a heptad repeat peptide derived from the S protein of Middle East respiratory syndrome coronavirus. *J. Virol.* **2013**, *87*, 13134-13140.

(17) Lau, Y.; De Andrade, P.; Wu, Y.; Spring, D. R. Peptide stapling techniques based on different macrocyclisation chemistries. *Chem. Soc. Rev.* **2015**, *44*, 91-102.

(18) Walensky, L. D.; Bird, G. H. Hydrocarbon-stapled peptides: principles, practice, and progress. *J. Med. Chem.* **2014**, *57*, 6275-6288.

(19) Tan, Y.; Lane, D. P.; Verma, C. S. Stapled peptide design: principles and roles of computation. *Drug Discov. Today* **2016**, *21*, 1642-1653.

(20) Kawamoto, S. A.; Coleska, A.; Ran, X.; Yi, H.; Yang, C.; Wang, S. Design of triazole-stapled BCL9 alpha-helical peptides to target the beta-Catenin/B-Cell CLL/lymphoma 9 (BCL9) protein-protein interaction. *J. Med. Chem.* **2012**, *55*, 1137-1146.

(21) Hojo, K.; Hossain, M. A.; Tailhades, J.; Shabanpoor, F.; Wong, L. L.L.; Ong-Palsson, E. E. K.; Kastman, H. E.; Ma, S.; Gundlach, A. L.; Rosengren, K. J.; Wade, J. D.; Bathgate, R. A. D. Development of a single-chain peptide agonist of the relaxin-3 receptor using hydrocarbon stapling. *J. Med. Chem.* **2016**, *59*, 7445-7456

(22) Frank, A. O.; Vangamudi, B.; Feldkamp, M. D.; Souza-Fagundes, E. M.; Luzwick, J. W.; Cortez, D.; Olejniczak, E. T.; Waterson, A. G.; Rossanese, O. W.; Chazin, W. J.; Fesik, S. W. Discovery of a potent stapled helix peptide that binds to the 70N domain of replication protein A. *J. Med. Chem.* **2014**, *57*, 2455-2461

(23) Hilinski, G. J.; Kim, Y. W.; Hong, J.; Kutchukian, P. S.; Crenshaw, C. M.; Berkovitch, S. S.; Chang, A.; Ham, S.; Verdine, G. L. Stitched alpha-helical peptides via bis ring-closing metathesis. *J. Am. Chem. Soc.* **2014**, *136*, 12314-12322.

(24) Chang, Y.; Graves, B.; Guerlavais, V.; Tovar, C.; Packman, K.; To, K. H.; Olson, K. A.; Kesavan, K.; Gangurde, P.; Mukherjee, A.; Baker, T.; Darlak, K.; Elkin, C.; Filipovic, Z.; Qureshi, F. Z.; Cai, H.; Berry, P.; Feyfant, E.; Shi, X. E.; Horstick, J.; Annis, D. A.; Manning, A. M.; Fotouhi, N.; Nash, H.; Vassilev, L. T.; Sawyer, T. K. Stapled alpha-helical peptide drug development: a potent dual inhibitor of MDM2 and MDMX for p53-dependent cancer therapy. *Proc. Natl. Acad. Sci. U. S. A.* **2013**, *110*, E3445-54.

(25) Wang, C.; Shi, W.; Cai, L.; Lu, L.; Wang, Q.; Zhang, T.; Li, J.; Zhang, Z.; Wang, K.; Xu, L.; Jiang, X.; Jiang, S.; Liu, K. Design, synthesis, and biological evaluation of highly potent

small molecule-peptide conjugates as new HIV-1 fusion inhibitors. *J. Med. Chem.* **2013**, *56*, 2527-2539.

(26) Wang, C.; Shi, W.; Cai, L.; Lu, L.; Yu, F.; Wang, Q.; Jiang, X.; Xu, X.; Wang, K.; Xu, L.; Jiang, S.; Liu, K. Artificial peptides conjugated with cholesterol and pocket-specific small molecules potently inhibit infection by laboratory-adapted and primary HIV-1 isolates and enfuvirtide-resistant HIV-1 strains. *J. Antimicrob. Chemother.* **2014**, *69*, 1537-1545.

(27) Wuo, M.; Mahon, A. B.; Arora, P. S. An effective strategy for stabilizing minimal coiled coil mimetics. *J. Am. Chem. Soc.* **2015**, *137*, 11618-11621.

(28) Apostolovic, B.; Danial, M.; Klok, H. A. Coiled coils: attractive protein folding motifs for the fabrication of self-assembled, responsive and bioactive materials. *Chem. Soc. Rev* .**2010**, *39*, 3541-3575.

(29) Zheng, B.; Wang, K.; Lu, L.; Yu, F.; Cheng, M.; Jiang, S.; Liu, K.; Cai, L. Hydrophobic mutations in buried polar residues enhance HIV-1 gp41 N-terminal heptad repeat-C-terminal heptad repeat interactions and C-peptides' anti-HIV activity. *AIDS* **2014**, *28*, 1251-1260.

(30) Qi, Z.; Shi, W.; Xue, N.; Pan, C.; Jing, W.; Liu, K.; Jiang, S. Rationally designed anti-HIV peptides containing multifunctional domains as molecule probes for studying the mechanisms of action of the first and second generation HIV fusion inhibitors. *J. Biol. Chem.* **2008**, *283*, 30376-30384.

(31) Anderhuber, N.; Fladischer, P.; Gruber-Khadjawi, M.; Mairhofer, J.; Striedner, G.; Wiltschi B. High-level biosynthesis of norleucine in E.coli for the economic labeling of proteins. *J. Biotechnol*. **2016**, *235*, 100-111.

(32) Fletcher, J. M.; Boyle, A. L.; Bruning, M.; Bartlett, G. J.; Vincent, T. L.; Zaccai, N. R.; Armstrong, C. T.; Bromley, E. H. C.; Booth, P. J.; Brady, R. L.; Thomson, A. R.; Woolfson, D.

N. A basis set of de novo coiled-coil peptide oligomers for rational protein design and synthetic biology. *ACS Synth. Biol.* **2012**, *1*, 240-250.

(33) Cotton, M.; Watson, S. J.; Zumla, A. I.; Makhdoom, H. Q.; Palser, A. L.; Ong, S. H.; Al Rabeeah, A. A.; Alhakeem, R. F.; Assiri, A.; Al-Tawfiq, J. A.; Albarrak, A.; Barry, M.; Shibl, A.; Alrabiah, F. A.; Hajjar, S.; Balkhy, H. H.; Flemban, H.; Rambaut, A.; Kellam, P.; Memish, Z. A. Spread, circulation, and evolution of the Middle East respiratory syndrome coronavirus. *mBio.* **2014**, *5*, e01062-13.

(34) Lawless, M. K.; Barney, S.; Guthrie, K. I.; Bucy, T. B.; Petteway, S. R.; Merutka, G. HIV-1 membrane fusion mechanism: structural studies of the interactions between biologically-active peptides from gp41. *Biochemistry* **1996,** *35*, 13697-13708.

(35) Cai, L. F.; Balogh, E.; Gochin, M. Stable extended human immunodeficiency virus type 1 gp41 coiled coil as an effective target in an assay for high-affinity fusion inhibitors, *Antimicrob. Agents Chemother.* **2009**, *53*, 2444-2449.

(36) Dwyer, J. J.; Wilson, K. L.; Davison, D. K.; Freel, S. A.; Seedorff, J. E.; Wring, S. A.; Tvermoes, N. A.; Matthews, T. J.; Greenberg, M. L.; Delmedico, M. K. Design of helical, oligomeric HIV-1 fusion inhibitor peptides with potent activity against enfuvirtide-resistant virus. *Proc. Natl. Acad. Sci. U. S. A.* **2007**, *104*, 12772-12777.

(37) Shi, W. G.; Cai, L. F.; Lu, L.; Wang, C.; Wang, K.; Xu, L.; Zhang, S.; Han, H.; Jiang, X. F.; Zheng, B. H.; Jiang, S. B.; Liu, K. L. Design of highly potent HIV fusion inhibitors based on artificial peptide sequences. *Chem. Commun.* **2012**, *48*, 11579-11581.

(38) Zhu, X. J.; Zhu, Y.; Ye, S.; Wang, Q.; Xu, W.; Su, S.; Sun, Z. W.; Yu, F.; Liu, Q.; Wang, C.; Zhang, T. H.; Zhang, Z. Q.; Zhang, X. Y.; Xu, J. Q.; Du, L. Y.; Liu, K. L.; Lu, L.; Zhang, R. G.;

Jiang, S. B. Improved pharmacological and structural properties of HIV fusion inhibitor AP3 over enfuvirtide: highlighting advantages of artificial peptide strategy. *Sci. Rep.* **2015**, *5*, 13028.

(39) Cui, H.; Qing, J.; Guo, Y.; Wang, Y.; Cui, L.; He, T.; Zhang, L.; Liu, L. Stapled peptide-based membrane fusion inhibitors of hepatitis C virus. *Bioorg. Med. Chem.* **2013**, *21*, 3547-3554.

(40) Liu, Q.; Xia, S.; Sun, Z.; Wang, Q.; Du, L.; Lu, L.; Jiang, S. Testing of Middle East respiratory syndrome coronavirus replication inhibitors for the ability to block viral entry. *Antimicrob. Agents Chemother*. **2015**, *59*, 742-744.

(41) Xia, S.; Liu, Q.; Wang, Q.; Sun, Z.; Su, S.; Du, L.; Ying, T.; Lu, L.; Jiang, S. Middle East respiratory syndrome coronavirus (MERS-CoV) entry inhibitors targeting spike protein. *Virus Res*. **2014**, *194*, 200-210.

(42) Zhao, G.; Du, L.; Ma, C.; Li, Y.; Li, L.; Poon, V. K.; Wang, L.; Yu, F.; Zheng, B. J.; Jiang, S.; Zhou, Y. A safe and convenient pseudovirus-based inhibition assay to detect neutralizing antibodies and screen for viral entry inhibitors against the novel human coronavirus MERS-CoV. *Virol. J*. **2013**, *10*, 266.

Table of Contents graphic